Applied Physics Letters

RESEARCH ARTICLE | NOVEMBER 16 2023

Studies on the nonlinear dielectric response in ferroelectric–dielectric composite system

Zixin Cao ; Yawei Li ; Liyan Shang ; Kai Jiang ; Jinzhong Zhang ; Liangqing Zhu ;
Zhigao Hu ; Junhao Chu

Appl. Phys. Lett. 123, 202905 (2023)
https://doi.org/10.1063/5.0175118

View Online

Export Citation

CrossMark

16 November 2023 14:27:15

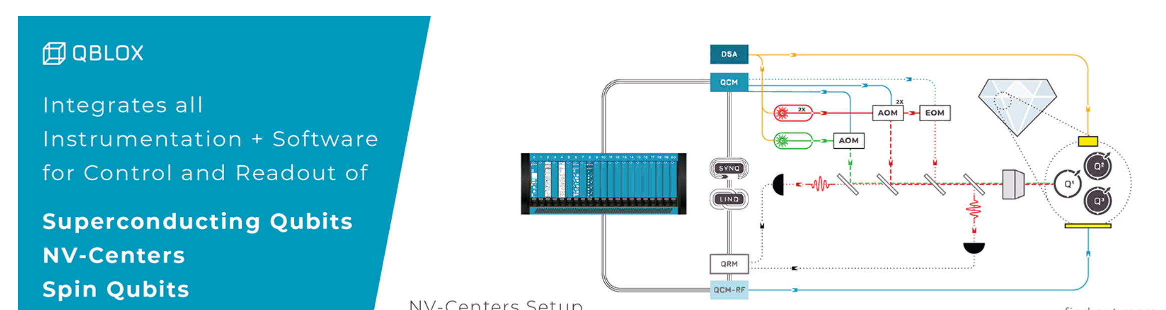

Applied Physics Letters ARTICLE pubs.aip.org/aip/apl

Studies on the nonlinear dielectric response in ferroelectric–dielectric composite system

Cite as: Appl. Phys. Lett. **123**, 202905 (2023); doi: 10.1063/5.0175118
Submitted: 5 September 2023 · Accepted: 4 November 2023 ·
Published Online: 16 November 2023

Zixin Cao,[1] Yawei Li,[1,a)] Liyan Shang,[1] Kai Jiang,[1] Jinzhong Zhang,[1] Liangqing Zhu,[1] Zhigao Hu,[1,2,a)] and Junhao Chu[1,2]

AFFILIATIONS

[1]Technical Center for Multifunctional Magneto-Optical Spectroscopy (Shanghai), Engineering Research Center of Nanophotonics and Advanced Instrument (Ministry of Education), Department of Physics, School of Physics and Electronic Science, East China Normal University, Shanghai 200241, China

[2]Collaborative Innovation Center of Extreme Optics, Shanxi University, Taiyuan 030006, China

[a)]Authors to whom correspondence should be addressed: ywli@ee.ecnu.edu.cn and zghu@ee.ecnu.edu.cn

ABSTRACT

The nonlinear dielectric response (NDR) of $Bi_{3.25}La_{0.75}Ti_3O_{12}$–$Al_2O_3$ systems has been studied. To reveal the effects of the dielectric layer (DL) systematically, a method based on the equivalent circuit analysis and parametric study is proposed. The consistency between the calculated results and the experimental results manifests the validity of the method. In addition to the Rayleigh coefficients varying monotonically with the capacitance of DL, it is revealed that the slope between the real and the imaginary parts of the complex capacitance under different ac voltages is related to the relative loss values of DL and the ferroelectric layer. The frequency dependence of the NDR parameters is also discussed. The method established in this work is useful for research on the devices based on the ferroelectric–dielectric system and the ultra-thin ferroelectric films.

Published under an exclusive license by AIP Publishing. https://doi.org/10.1063/5.0175118

16 November 2023 14:27:15

Ferroelectric materials have attracted tremendous attention due to their potential applications in nonvolatile memories, artificial synapses, and energy storage.[1–4] The ferroelectric performances originate from the development of domains and the displacement of domain walls under the electric field. The nonlinear dielectric response (NDR) has been used to characterize domain-related processes since Taylor and co-workers proved the contribution of domain walls to the permittivity of $Pb(Zr_x,Ti_{1-x})O_3$ (PZT).[5,6] According to NDR, the relationship between the real part (ε') of the complex permittivity and the ac electric field is given by the Rayleigh law,[6]

$$\varepsilon'(E_0) = \varepsilon'_{in} + \alpha E_0, \tag{1}$$

where E_0 is the amplitude of the ac field. The initial permittivity ε'_{in} represents the reversible component in the permittivity, and the Rayleigh coefficient α represents the irreversible contribution from the movement of domain walls. Moreover, the imaginary part (ε'') of the complex permittivity also changes with the ac field and follows:[7]

$$\varepsilon''(E_0) = 4\alpha E_0/3\pi. \tag{2}$$

From (1) and (2), the relationship between ε' and ε'' can be rewritten as

$$\varepsilon' = \varepsilon'_{in} + 3\pi\varepsilon''/4. \tag{3}$$

It means that ε' changes linearly with ε'', and the slope k should be $3\pi/4$. However, the reported values of α are quite different, and deviations of k from $3\pi/4$ have been observed in many ferroelectrics.[7–15] Some mechanisms, such as the electrode effect and the orientation of films, have been proposed to explain these phenomena.[5]

For devices based on the ferroelectric films, the non-ferroelectric interfacial layer between the ferroelectric layer (FL) and the electrodes, which is the so-called dead layer, has a significant impact on the performances of the devices, such as the reduction of the permittivity and the polarization.[16,17] Alternatively, novel phenomena, such as the negative capacitance effect and the excellent energy storage performances, are observed in the ferroelectric–dielectric (FE–DE) composite system.[2,18,19] Therefore, studies on the FE–DE composite system will reveal the mechanism and extend the applications of the ferroelectric devices. However, few research works on NDR in the FE–DE system were reported. In addition, the dielectric layer (DL) is always considered as an ideal capacitor, and the simple model of the series capacitor is often used in most published literature.[16,17] The influence of the dielectric loss cannot be considered by this model. In this work, the artificial FE–DE structures formed by the $Bi_{3.25}La_{0.75}Ti_3O_{12}$ film and

Published under an exclusive license by AIP Publishing

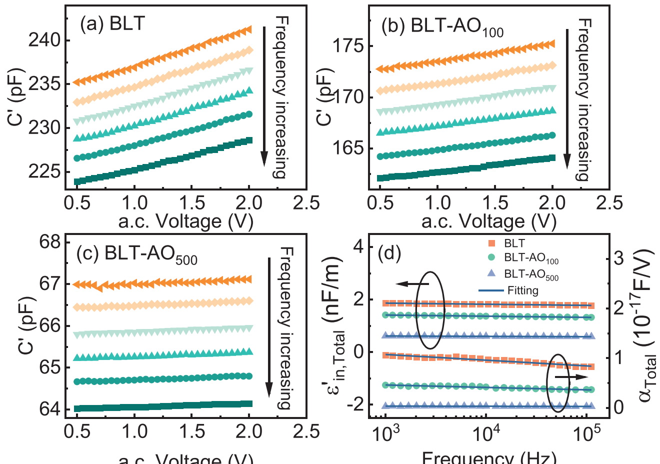

FIG. 1. The ac voltage dependence of the capacitance for (a) BLT, (b) BLT–AO_{100}, and (c) BLT–AO_{500}. (d) The frequency dependence of $\varepsilon'_{in,Total}$ and α_{Total}.

Al_2O_3 films are fabricated, and the NDR is studied experimentally. A method based on the equivalent circuit analysis and parametric study is established to reveal the effects of DL on the NDR parameters.

The $Bi_{3.25}La_{0.75}Ti_3O_{12}$ films were prepared on $Pt/Ti/SiO_2/Si$ substrates by the sol–gel method and then covered by the amorphous Al_2O_3 films fabricated by atomic layer deposition (ALD) technology with 100 and 500 ALD cycles. The samples were denoted as BLT, BLT–AO_{100}, and BLT–AO_{500}. Furthermore, Al_2O_3 films with 100 and 500 ALD cycles were also deposited on $Pt/Ti/SiO_2/Si$ substrates and denoted as AO_{100} and AO_{500}, respectively. The thicknesses of BLT, AO_{100}, and AO_{500} were 320, 9, and 45 nm, respectively, obtained by the spectroscopic ellipsometry. Au top electrodes with the diameter of 200 μm were sputtered for the electrical measurements. The dielectric responses of the samples were measured by a dielectric analyzer (Alpha-A, Novocontrol Technologies) in the ac voltage range 0.5–2 V and the frequency range 1–100 kHz. Both the parameters of NDR, including the Rayleigh coefficient α, the slope k, and the initial permittivity ε'_{in} can be deduced from the dependence of the complex capacitance on the oscillating voltage (C-OSC), and the geometry size of the samples were taken into account.

As shown in Figs. 1(a)–1(c), the real part (C') of the complex capacitance increases approximately linearly with the amplitude of the ac voltage and decreases with the frequency for the samples. Figure 1(d) exhibits the frequency dependence of the initial permittivity and the Rayleigh coefficient obtained by fitting the curves in Figs. 1(a)–1(c) using Eq. (1). The derived initial permittivity and Rayleigh coefficient are the total equivalent values of the stack. They are denoted as $\varepsilon'_{in,Total}$ and α_{Total}. Both $\varepsilon'_{in,Total}$ and α_{Total} decrease linearly with the logarithm of the frequency. Similar phenomena have also been observed in other ferroelectrics such as $Pb(Yb_{1/2}Nb_{1/2})O_3$-$PbTiO_3$.[6] Nattermann *et al.* have theoretically presented the dependence of the susceptibility on the logarithm of the frequency in disorder system and explained the pinning of the magnetic domain wall.[20] Thereafter, this mechanism is used to explain the pinning of the ferroelectric domain wall.[21–23] The frequency dependence of $\varepsilon'_{in,Total}$ and α_{Total} can be depicted as

$$\begin{aligned} \varepsilon'_{in,Total} &= e_0 - e\ln(\omega), \\ \alpha_{Total} &= a_0 - a\ln(\omega). \end{aligned} \tag{4}$$

The fitting results of the curves in Fig. 1(d) by Eq. (4) are exhibited in Table I.

It is manifested from Fig. 1(d) that both $\varepsilon'_{in,Total}$ and α_{Total} decrease with the Al_2O_3 thickness increasing. The Rayleigh coefficient is generally considered to be related to the distribution of the potential barriers that hinder the movement of domain walls in ferroelectrics.[24–26] It is decided by the ferroelectrics. However, when the Rayleigh coefficient is derived from the experimentally measured capacitance, the obtained value is influenced by the existence of the non-ferroelectric interfacial layer, which results in the deviation of the measured capacitance from that of the pure ferroelectric capacitor, just like those demonstrated in this work.

To further investigate the influence of DL on NDR, the relationship between the real part and the imaginary part (C'') of the complex capacitance is considered. According to Eq. (3), the relationship between C' and C'' follows:

$$C' = C'_{in} + kC'', \tag{5}$$

and k should be $3\pi/4$. Figures 2(a)–2(c) display the curves in the complex capacitance plane. Both C' and C'' decrease when the thickness of the Al_2O_3 film increases. This feature accords with the Kramers–Kronig relations.[27] The linear relationship between C' and C'' for the samples can be observed. The fitted initial capacitance $C'_{in,Total}$ and k_{Total} for the total stack by Eq. (5) is shown in Fig. 2(d). The variations of $C'_{in,Total}$ with frequency and DL thickness are consistent with those of $\varepsilon'_{in,total}$ in Fig. 1(d). Moreover, k_{Total} decreases with the thickness of DL increasing and is larger than the theoretical value of $3\pi/4$. The experimental results indicate that the existence of DL also influences k_{Total}. Because k_{Total} relates to the imaginary part of the complex capacitance and cannot be deduced by the series capacitor model, a method based on the equivalent circuit model and the parametric study is proposed to investigate the effect of DL.

The total complex capacitance (C^*_{Total}) of a circuit composed of two components connected in series is

TABLE I. Fitting results of the samples.

Sample ID	e_0 (nF/m)	e (nF s/m rad)	a_0 (10^{-18} F/V)	a (10^{-18} F s/V rad)
BLT	2.028 ± 0.001	0.0184 ± 0.0001	15.104 ± 0.004	0.498 ± 0.004
BLT–AO_{100} (Exp.)	1.577 ± 0.001	0.0188 ± 0.0001	6.471 ± 0.003	0.212 ± 0.004
BLT–AO_{100} (Cal.)	1.3840 ± 0.0003	0.02822 ± 0.00005	6.165 ± 0.003	0.267 ± 0.003
BLT–AO_{500} (Exp.)	0.6678 ± 0.0004	0.00593 ± 0.00005	0.491 ± 0.003	0.014 ± 0.002
BLT–AO_{500} (Cal.)	0.6462 ± 0.0002	0.01531 ± 0.00003	1.268 ± 0.001	0.058 ± 0.001

16 November 2023 14:27:15

Published under an exclusive license by AIP Publishing

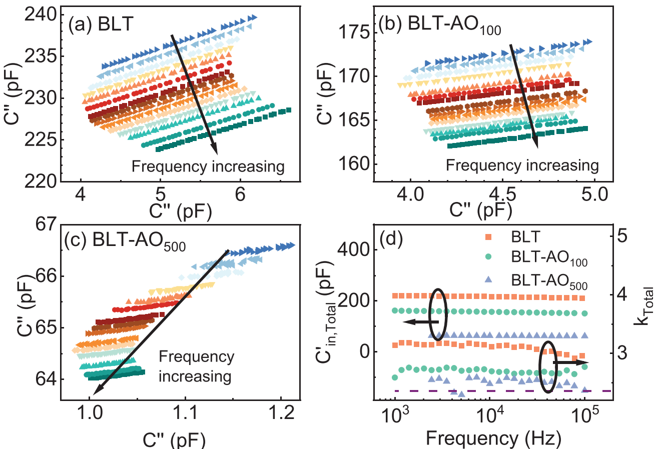

FIG. 2. C' vs C'' for (a) BLT, (b) BLT–AO_{100}, and (c) BLT–AO_{500}. (d) The frequency dependence of $C'_{in,Total}$ and k_{Total}. The dash line in (d) is the position of $3\pi/4$. The absence of the data for BLT–AO_{500} in the lower frequency region is because the excessive noise hinders the fitting of the experimental data.

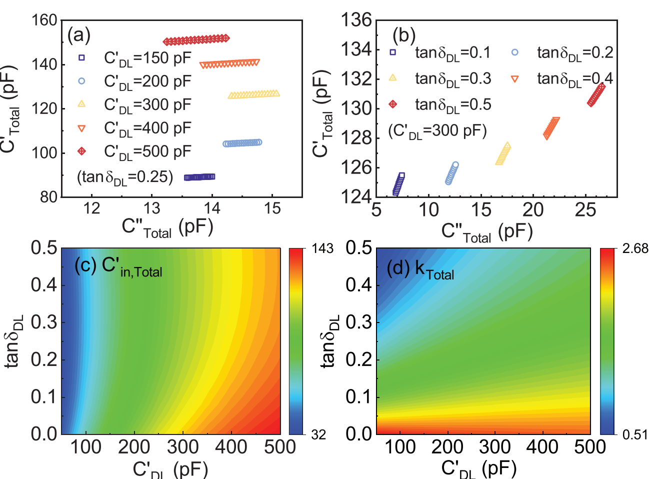

FIG. 3. Relationship between C'_{Total} and C''_{Total} with different (a) C'_{DL} and (b) $\tan\delta_{DL}$. Mapping diagrams of (c) $C'_{in,Total}$ and (d) k_{Total}.

$$C^*_{Total} = 1/\left(j\omega Z^*_{Total}\right) = 1/\left[j\omega\left(Z^*_{FL} + Z^*_{DL}\right)\right], \tag{6}$$

where Z^*_{Total} is the total complex impedance of the circuit, Z^*_{FL} and Z^*_{DL} are the complex impedance of FL and DL, respectively, and ω is the circular frequency. The complex capacitance of FL follows Eq. (3) and can be expressed as

$$C'_{FL} = C'_{in,FL} + k_{FL}C''_{FL}, \tag{7}$$

where C'_{FL} and C''_{FL} are the real and imaginary parts of the complex capacitance of FL, respectively, $C'_{in,FL}$ and k_{FL} are the initial capacitance and the slope of FL, respectively. Based on Eqs. (6) and (7), C^*_{Total} is rewritten as

$$C^*_{Total} = C'_{Total} - jC''_{Total} = \frac{C'^2_{in,FL}C''_{DL} + 2C'_{in,FL}C''_{DL}k_{FL}C''_{FL} + C''_{FL}\left\{C'^2_{DL} + C''_{DL}\left[C''_{DL} + C''_{FL}\left(1+k^2_{FL}\right)\right]\right\}}{\left(C''_{DL}+C''_{FL}\right)^2 + \left(C'_{in,FL} + C'_{DL} + k_{FL}C''_{FL}\right)^2} - j\frac{C'^2_{in,FL}C'_{DL} + C'_{in,FL}\left(C'^2_{DL} + C''^2_{DL} + 2k_{FL}C'_{DL}C''_{FL}\right) + C''_{FL}\left[k_{FL}\left(C'^2_{DL}+C''^2_{DL}\right) + C'_{DL}C''_{FL}\left(1+k^2_{FL}\right)\right]}{\left(C''_{DL}+C''_{FL}\right)^2 + \left(C'_{in,FL} + C'_{DL} + k_{FL}C''_{FL}\right)^2}, \tag{8}$$

where C'_{DL} and C''_{DL} are the real and imaginary parts of the complex capacitance of DL, respectively. The initial capacitance $C'_{in,Total}$ and the slope k_{Total} of the total circuit can be obtained if C'_{Total} is linearly dependent on C''_{Total}.

In the first segment of the parametric study, the parameters of $C'_{in,FL} = 200$ pF, $k_{FL} = 3\pi/4$, and C''_{FL} between 5 and 6.5 pF are used to generate the data of FL following Eq. (5). Figures 3(a) and 3(b) exhibit the calculated results on the relationship between C'_{Total} and C''_{Total} with different C'_{DL} and $\tan\delta_{DL}$, where $\tan\delta_{DL}$ is the loss tangent of DL and defined as the ratio of the imaginary and real parts of the complex permittivity. It is clear that C'_{Total} varies linearly with C''_{Total}. The derived $C'_{in,Total}$ and k_{Total} are displayed in Figs. 3(c) and 3(d), respectively. $C'_{in,Total}$ increases with C'_{DL}, but the variation of $C'_{in,Total}$ with $\tan\delta_{DL}$ is not monotonous. As shown in Fig. 3(c), when $\tan\delta_{DL}$ is lower, $C'_{in,Total}$ decreases with $\tan\delta_{DL}$ increasing. The trend is inverse when $\tan\delta_{DL}$ is higher. In contrast with $C'_{in,Total}$, different changes of k_{Total} can be observed from Figs. 3(b) and 3(d). k_{Total} decreases with $\tan\delta_{DL}$ increasing but changes non-monotonically with C'_{DL}. When $\tan\delta_{DL} < 0.03$, k_{Total} is higher than the value of k_{FL} ($3\pi/4$) and decreases gradually toward $3\pi/4$ with C'_{DL} increasing, which corresponds to the DL thickness decreasing. Nevertheless, k_{Total} is lower than $3\pi/4$ when $\tan\delta_{DL} \geq 0.03$ and closes up to $3\pi/4$ with C'_{DL} increasing. The results of the parametric study indicate that the value 0.03 for $\tan\delta_{DL}$ is a demarcation point. According to the parameters that are used for the parametric study, the loss of FL is about 0.03. This means that k_{Total} is not only determined by the capacitance of FL and DL but also related to the relative value of the losses of FL and DL. Therefore, it can be inferred that the reported values of k may be influenced by the interfacial layer between the ferroelectrics and the electrodes.[7,14,15]

In the second segment of the parametric study, the influence of DL on the frequency dependence of the composite structure is studied. The experimental C-OSC results of BLT film are used as the parameters of FL. DL is represented by a parallel connection unit composed of a resistor and a constant phase element (CPE). The complex capacitance of this parallel unit can be expressed as[10]

$$C^*_{R-CPE} = Y_0\omega^{n-1}\sin(n\pi/2) - j\frac{1 + RY_0\omega^n\cos(n\pi/2)}{R\omega}, \tag{9}$$

where R is the resistance, Y_0 represents the pseudo-capacitance, and n is the exponent. $C^*_{R\text{-}CPE}$ with different R, Y_0, n, and ω is calculated by

16 November 2023 14:27:15

Published under an exclusive license by AIP Publishing

Eq. (9), and the corresponding C'_{DL} and $\tan\delta_{DL}$ are used to research the effects of DL on the NDR parameters.

The calculated frequency spectra are exhibited in Fig. 4. C'_{DL} and $\tan\delta_{DL}$ of R-CPE with different R are shown in Figs. 4(a) and 4(b), which represent the case that a ferroelectric capacitor connects in series with the elements that possess same capacitance and different leakage. Neither the frequency nor the resistance affects C'_{DL}. $\tan\delta_{DL}$ decreases with the frequency increasing and correlates with R negatively. The spectra of $C'_{in,Total}$ and k_{Total} are displayed in Figs. 4(c) and 4(d). Compared with BLT, the existence of R-CPE leads to the decrease in $C'_{in,Total}$. In Fig. 4(c), the influence of R mainly appears in the low-frequency region. It is related to the significant increase in $\tan\delta_{DL}$ in Fig. 4(b). Higher loss in the low-frequency region results in the larger reduction of $C'_{in,Total}$, especially for the case of $R = 1\times10^{7}$ Ω. Most of the calculated k_{Total} are higher than the measured k of BLT. It is because the corresponding $\tan\delta_{DL}$ (in the full frequency region of $R = 4\times10^{7}$, 1×10^{8}, and 1×10^{9} Ω and the high-frequency region of $R = 1\times10^{7}$ Ω) of the R-CPE is lower than 0.03. On the contrary, for $R = 1\times10^{7}$ Ω, $\tan\delta_{DL}$ in the low-frequency region is higher than 0.03. It leads to lower k_{Total} than that of BLT. For the R-CPE, the lower value of R means the leakage current in DL is higher. The calculated results in Fig. 4(d) reveal that the influences of the leakage in DL on k_{Total} cannot be ignored until the resistance of DL is higher than 10^{8} Ω.

The influences of Y_0 are shown in Figs. 4(e)–4(h). C'_{DL} does not change with frequency but varies with Y_0 because the greater Y_0 causes the higher equivalent capacitance. Moreover, $\tan\delta_{DL}$ is negatively correlated with Y_0 although it still decreases when the frequency increases. These effects are opposite to those of R. The curves of $C'_{in,Total}$ and k_{Total} are shown in Figs. 4(g) and 4(h), respectively. The influence of the lower $\tan\delta_{DL}$ on $C'_{in,Total}$ and k_{Total} mainly follows the trend in the region where $\tan\delta_{DL}$ is less than 0.03 in the mapping diagrams in Fig. 3. In Fig. 4(g), the $C'_{in,Total}$ curves are beneath that of the pure BLT and drop further with C'_{DL} decreasing. However, the k_{Total} curves in Fig. 4(h) are above that of the pure BLT and further increase with the decrease in C'_{DL}. For $n = 1$, the CPE is equivalent to a capacitor. The calculated results indicate that the influence produced by an interfacial layer with excellent insulation can be regarded as that produced by an ideal capacitor. The linear relationship between the reciprocals of $C'_{in,Total}$ and that of Y_0 in the inset of Fig. 4(g) manifests that the result follows the model that an ideal capacitor connects with the BLT in series.

The effects of n are displayed in Figs. 4(i)–4(l). Different from the case of $n = 1$ in which C'_{DL} does not change with the frequency, C'_{DL} decreases with the increase in frequency when $n < 1$. The smaller the value of n, the greater the curves of C'_{DL} decline. The relationship between C'_{DL} and frequency is linear in double logarithmic coordinates, as shown in Fig. 4(i). $\tan\delta_{DL}$ decreases with the frequency increasing. The decrease in n results in the rapid rise of $\tan\delta_{DL}$, as exhibited in Fig. 4(j). The excessively higher $\tan\delta_{DL}$ means that the ac conductance in CPE is greater because $\tan\delta_{DL}$ is related to C''_{DL}, which is proportional to the real part of the complex admittance. Therefore, the decline of $C'_{in,Total}$ with the decrease in n can be attributed to both the decrease in C'_{DL} and the increase in $\tan\delta_{DL}$, as shown in Fig. 4(k). According to the curves in Fig. 4(j), except for the case $n = 1$, the values of $\tan\delta_{DL}$ are higher than 0.03 in the cases $n = 0.95$, 0.9, and 0.7.

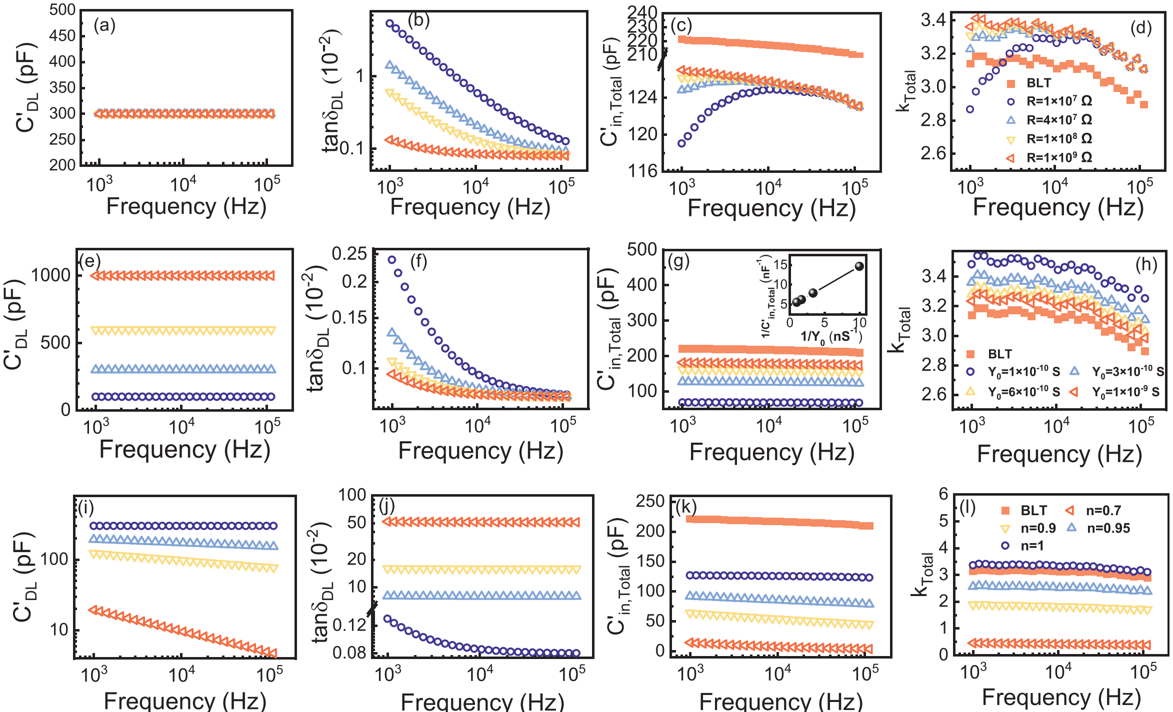

FIG. 4. The calculated frequency spectra of (a), (c), and (i) C'_{DL}, (b), (f), and (j) $\tan\delta_{DL}$ of R-CPE, (c), (g), and (k) $C'_{in,Total}$, and (d), (h), and (l) k_{Total} of the composite system. (a)–(d) $Y_0 = 3\times10^{-10}$ S and $n = 1$ with different R. (e)–(h) $R = 1\times10^{9}$ Ω and $n = 1$ with different Y_0. (i)–(l) $R = 1\times10^{9}$ Ω and $Y_0 = 3\times10^{-10}$ S with different n. The inset of (g) shows $1/C'_{in,Total}$ vs $1/Y_0$.

16 November 2023 14:27:15

Published under an exclusive license by AIP Publishing

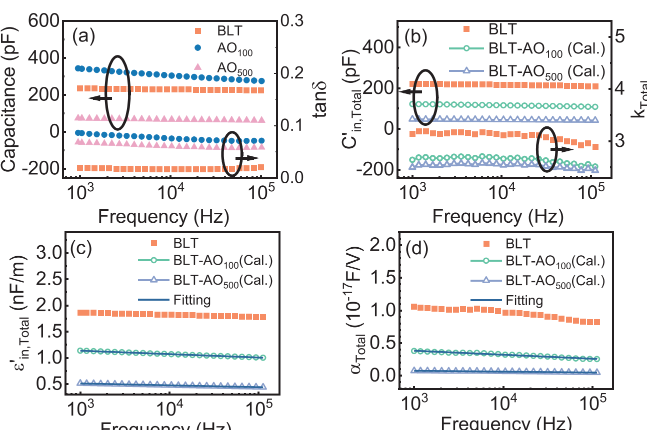

FIG. 5. (a) The capacitance and loss spectra of BLT and Al_2O_3 films. (b) The frequency dependence of $C'_{in,Total}$ and k_{Total} of BLT–AO_{100} and BLT–AO_{500} from the calculated complex capacitance. The frequency spectra of the total equivalent (c) $\varepsilon'_{in,Total}$ and (d) α_{Total} are derived from the calculated C-OSC results. The experimental results of BLT are also plotted in (b)–(d).

Therefore, the values of k_{Total} are lower than that of BLT and decrease significantly with n, except for the case $n = 1$, as shown in Fig. 4(l).

Finally, the experimental data and the model are used conjunctly to research the NDR in our BLT–Al_2O_3 system. According to the calculated results, k_{Total} of BLT–AO_{100} and BLT–AO_{500} lower than that of BLT in Fig. 2(d) implies that the loss of the Al_2O_3 layer is higher than that of the BLT layer in the composite system. In general, the experimental data for a dead layer are not available. In our work, the experimental data of the Al_2O_3 films on Pt electrode are used. The experimental capacitance and loss spectra of BLT, AO_{100}, and AO_{500} are displayed in Fig. 5(a). The loss of BLT is smaller than 0.025, and those of AO_{100} and AO_{500} are higher than 0.05. The capacitance and loss of AO_{100} and AO_{500} in Fig. 5(a) are fitted by Eq. (9), and the fitting results of R, Y_0, and n are 3.93×10^7 Ω, 5.20×10^{-10} S, and 0.95, and 2.51×10^8 Ω, 1.03×10^{-10} S, and 0.96 for AO_{100} and AO_{500}, respectively. These fitting results and the experimental data of BLT are taken into Eq. (8). The calculated $C'_{in,Total}$ and k_{Total} from the linear relationship between C' and C'' are shown in Fig. 5(b). The results in Fig. 5(b) are similar to the experimental results in Fig. 2(d). Both $C'_{in,Total}$ and k_{Total} decrease with the Al_2O_3 thickness increasing. Based on the calculated results, the smaller k_{Total} and $C'_{in,Total}$ than those of BLT is decided by the capacitance and the loss of the Al_2O_3, especially for the case of AO_{100} which resistance is lower than 10^8 Ω. The effects of DL on α_{Total} are also calculated by our method. The frequency dependence of $\varepsilon'_{in,total}$ and α_{Total} obtained from the calculated C-OSC data is plotted in Figs. 5(c) and 5(d), respectively. The curves exhibit the same trends as the experimental results shown in Fig. 2(d). The fitting results of the calculated curves according to Eq. (4) are also listed in Table I. Compared with BLT–AO_{100}, the difference between the experimental and the calculated results for BLT–AO_{500} is higher, which can be ascribed to the smaller capacitance of the AO_{500}. The consistency between the experimental and calculated results indicates that our method is appropriate for the studies on NDR in the FE–DE composite system. According to the experimental and calculated results, the NDR parameters in the FE–DE composite system are affected by both the capacitance and the loss of DL and FL, especially when DL is very thin. This work will be significant for the devices based on ultra-thin ferroelectric films and composite systems.

This work was supported by the National Key Research and Development Program of China (No. 2019YFB2203403), the Natural Science Foundation of China (Nos. 62090013, 62074058, 61974043, and 61974044), the Projects of Science and Technology Commission of Shanghai Municipality (Nos. 21JC1402100 and 19511120100), the Program for Professor of Special Appointment (Eastern Scholar) at Shanghai Institutions of Higher Learning, and the Fundamental Research Funds for the Central Universities.

AUTHOR DECLARATIONS

Conflict of Interest

The authors have no conflicts to disclose.

Author Contributions

Zixin Cao: Data curation (equal); Investigation (equal); Visualization (equal); Writing – original draft (equal). **Yawei Li:** Conceptualization (equal); Data curation (equal); Investigation (equal); Methodology (equal); Writing – original draft (equal). **Liyan Shang:** Data curation (equal); Investigation (equal); Writing – original draft (equal). **Kai Jiang:** Investigation (equal); Methodology (equal); Writing – review & editing (equal). **Jinzhong Zhang:** Conceptualization (equal); Visualization (equal); Writing – review & editing (equal). **Liangqing Zhu:** Data curation (equal); Methodology (equal); Writing – review & editing (equal). **Zhigao Hu:** Funding acquisition (equal); Methodology (equal); Supervision (equal); Writing – review & editing (equal). **Junhao Chu:** Conceptualization (equal); Supervision (equal); Writing – review & editing (equal).

DATA AVAILABILITY

The data that support the findings of this study are available from the corresponding authors upon reasonable request.

REFERENCES

[1]H. F. Liu, T. Q. Lu, Y. X. Li, Z. Y. Ju, R. T. Zhao, J. Z. Li, M. H. Shao, H. N. Zhang, R. R. Liang, X. R. Wang, R. Guo, J. S. Chen, Y. Yang, and T. L. Ren, Adv. Sci. **7**(19), 2001266 (2020).
[2]N. F. Mao, L. H. Meng, Y. W. Li, Z. G. Hu, and J. H. Chu, Ceram. Int. **47**(6), 7720 (2021).
[3]Z. N. Xi, J. J. Ruan, C. Li, C. Y. Zheng, Z. Wen, J. Y. Dai, A. D. Li, and D. Wu, Nat. Commun. **8**, 15217 (2017).
[4]S. T. Yang, X. Y. Li, T. L. Yu, J. Wang, H. Fang, F. Nie, B. He, L. Zhao, W. M. Lü, S. S. Yan, A. Nogaret, G. Liu, and L. M. Zheng, Adv. Funct. Mater. **32**(35), 2202366 (2022).
[5]A. Bernal and N. Bassiri-Gharb, Appl. Phys. Lett. **95**(4), 042902 (2009).
[6]D. V. Taylor and D. Damjanovic, J. Appl. Phys. **82**(4), 1973 (1997).
[7]J. E. García, R. Pérez, and A. Albareda, J. Phys.: Condens. Matter **17**(44), 7143 (2005).
[8]D. Wu, G. L. Yuan, and A. D. Li, Appl. Phys. Lett. **90**(6), 062902 (2007).
[9]Y. Guan, D. Y. Zhou, J. Xu, X. H. Liu, F. Cao, X. L. Dong, J. Müller, T. Schenk, and U. Schroeder, Phys. Status Solidi RRL **9**(10), 589 (2015).
[10]T. Schenk, M. Hoffmann, M. Pešić, M. H. Park, C. Richter, U. Schroeder, and T. Mikolajick, Phys. Rev. Appl. **10**(6), 064004 (2018).
[11]S. Bhattacharyya, S. Saha, and S. B. Krupanidhi, Thin Solid Films **422**(1–2), 155 (2002).

16 November 2023 14:27:15

Published under an exclusive license by AIP Publishing

[12]M. Ye, H. T. Huang, T. Li, S. M. Ke, P. Lin, B. L. Peng, M. F. Mai, Q. Sun, X. Peng, and X. R. Zeng, Appl. Phys. Lett. **107**(20), 202902 (2015).
[13]X. J. Lou, H. J. Zhang, Z. D. Luo, F. P. Zhang, Y. Liu, Q. D. Liu, A. P. Fang, B. Dkhil, M. Zhang, X. B. Ren, and H. L. He, Appl. Phys. Lett. **105**(10), 102907 (2014).
[14]J. E. García, R. Pérez, D. A. Ochoa, A. Albareda, M. H. Lente, and J. A. Eiras, J. Appl. Phys. **103**(5), 054108 (2008).
[15]J. E. García, J. D. S. Guerra, E. B. Araújo, and R. Pérez, J. Phys. D **42**(11), 115421 (2009).
[16]J. Wang, Y. F. Xia, L. Q. Chen, and S. Q. Shi, J. Appl. Phys. **110**(11), 114111 (2011).
[17]Y. F. Xia and J. Wang, Smart Mater. Struct. **21**(9), 094019 (2012).
[18]C. S. Hsu, S. C. Chang, D. E. Nikonov, I. A. Young, and A. Naeemi, Phys. Rev. Appl. **15**(3), 034048 (2021).
[19]X. Y. Zhao, K. L. Zhang, K. Hu, Y. J. Zhang, Q. Z. Zhou, Z. H. Wang, Y. She, Z. Z. Zhang, and F. Wang, IEEE Trans. Electron Devices **68**(12), 6100 (2021).
[20]T. Nattermann, Y. Shapir, and I. Vilfan, Phys. Rev. B **42**(13), 8577 (1990).
[21]N. B. Gharb and S. Trolier-McKinstry, J. Appl. Phys. **97**(6), 064106 (2005).
[22]W. Kleemann, J. Dec, S. Miga, T. Woike, and R. Pankrath, Phys. Rev. B **65**(22), 220101 (2002).
[23]V. Mueller, Y. Shchur, H. Beige, A. Fuith, and S. Stepanow, Europhys. Lett. **57**(1), 107 (2002).
[24]D. Bolten, U. Böttger, T. Schneller, M. Grossmann, O. Lohse, and R. Waser, Appl. Phys. Lett. **77**(23), 3830 (2000).
[25]O. Boser, J. Appl. Phys. **62**(4), 1344 (1987).
[26]Y. W. Li, J. L. Sun, J. Chen, X. J. Meng, and J. H. Chu, Appl. Phys. Lett. **87**(18), 182902 (2005).
[27]R. Lovell, J. Phys. C **7**(23), 4378 (1974).

16 November 2023 14:27:15

Published under an exclusive license by AIP Publishing